P5.4 MODIFICATION OF THE WIND−DRIVEN CIRCULATION AND STRATIFIED SPIN−UP AT OCEAN FRONTS

Leif N. Thomas* and Peter B. Rhines

School of Oceanography, University of Washington, Seattle, Washington

1. INTRODUCTION

The occurrence of enhanced upper−ocean meridional density gradients in the Subtropical Convergence Zone (STCZ) has long been associated with Ekman frontogenesis, a process in which surface density gradients are intensified by convergent Ekman transport. However, based on data obtained during the FASINEX experiment by Halliwell et al 1991 (H91), the direct connection between subtropical fronts and Ekman convergence is not obvious, as H91 showed that the magnitude of the convergence of the Ekman transport was too small to explain the formation and maintenance of observed fronts. The spatial resolution of the wind−stress field used in this calculation was coarse, poorly resolving winds with lengthscales less than several hundred kilometers. Friehe et al 1991 using aircraft measurements of turbulence in the marine atmospheric boundary layer made during the FASINEX experiment demonstrated that wind−stress varied by O(0.1 N m^{-2}) over the width of the front O(20 km). This significant reduction in lengthscale of wind−stress implies that the wind−stress curl and hence Ekman convergence used in H91 was underestimated. A nondimensional measure of the strength of Ekman convergence is the Rossby number $\epsilon = \tau_o / \rho_o f^2 \delta_e L$ where τ_o is the magnitude of the wind−stress, ρ_o is the reference density, f is the Coriolis parameter, δ_e is the thickness of the Ekman layer, and L is the lengthscale of the wind. If we suppose that $\delta_e \sim$ 30 m, with f=6.6x10^{-5} s^{-1} the Rossby number is $\epsilon = 0.04$. Using a weakly nonlinear analytical theory along with two−dimensional, nonhydrostatic numerical simulations we will show that winds yielding such Rossby numbers generate fronts in a reasonable amount of time, and suggests that Ekman frontogenesis may still be a viable theory for explaining the predominance of fronts in the STCZ.

Corresponding author address: Leif Thomas, School of Oceanography, University of Washington, Box 357490, Seattle Washington 98195−7940, email: leif@ocean.washington.edu

2. NONLINEAR STRATIFIED SPIN−UP

The theoretical model is based on nonlinear stratified spin−up theory (NSSU), Thomas and Rhines 2001 (TR). NSSU is an extension of the classic theory of stratified spin−up (SSU) (see Allen 1973 and references therein) to include the effect of the nonlinear modification of the Ekman transport by the vertical vorticity generated during the spin−up of the fluid. SSU describes the acceleration of a rotating, stratified fluid by a secondary circulation driven by convergences and/or divergences of the Ekman transport. Due to the Coriolis force, the horizontal motions associated with this circulation will continually accelerate a flow perpendicular to the secondary circulation, while the vertical motions will advect the density field. This process occurs with a timescale of order $\tau_h = E^{-1/2} f^{-1}$ (where $E = (\delta_e / H)^2$ is the Ekman number and H is the total depth of the fluid) which is long compared to the time required for geostrophic adjustment, hence during SSU the downwind velocity is in a thermal−wind balance. For the case of a wind−stress curl constant in time, SSU generates an interior geostrophic flow in the direction of the wind that grows linearly with time. At some time, the magnitude of the geostrophic flow becomes strong enough to effect the dynamics of the flow in the Ekman layer and horizontal advection of momentum must be retained in an analysis of the velocity in the Ekman layer. When this is done, the Ekman transport M is found to vary inversely with the absolute vorticity rather than the planetary vorticity (Stern 1965; and Niiler 1969):

$$M = \frac{\tau}{\rho_o (f + \zeta)} \tag{1}$$

where τ is the wind−stress, $\zeta = \partial v / \partial x$ is the vertical component of the relative vorticity of the geostrophic flow v , and x is the

coordinate perpendicular to the wind. Consequently Ekman pumping/suction:

$$w_e = \frac{1}{\rho_o (f+\zeta)} \frac{\partial \tau}{\partial x} - \frac{\tau}{\rho_o (f+\zeta)^2} \frac{\partial \zeta}{\partial x} \qquad (2)$$

can occur even if the wind−stress does not have a curl, as a result of spatial variations in the vertical vorticity, i.e. the second term in (2). More important to NSSU is the first term of (2) which implies that Ekman pumping induced by the curl of the wind−stress is amplified (reduced) in regions of anticyclonic (cyclonic) vorticity. The essence of NSSU is as follows: as vertical vorticity is generated during the spin−up of the fluid by the secondary circulation, the vertical vorticity feeds back on the Ekman pumping/suction, enhancing pumping and reducing suction. This is because Ekman pumping is correlated with anticyclonic vorticity whereas Ekman suction is correlated with cyclonic vorticity. This feedback mechanism causes anticyclonic vorticity to grow more rapidly than cyclonic vorticity.

This mechanism was investigated in TR for the case of an initially quiescent, uniformly stratified fluid (with buoyancy frequency N^2) forced by a wind−stress: $\vec{\tau} = \tau_o \cos(2\pi x/L)\hat{j}$, where $\hat{j}$ is the unit vector in the *y*−direction. The analysis was accomplished by the use of a regular perturbation expansion in orders of the Rossby number ϵ for flow quantities within the Ekman layer and in the interior of the fluid. For example, the interior velocity in the *y*−direction was expanded as follows;

$$v_i = U(v_i^{(1)}(x,z,\bar{t},S) + \epsilon v_i^{(2)}(x,z,\bar{t},S) + \ldots) \qquad (3)$$

where $U = \tau_o/\rho_o f \delta_e$ is the characteristic horizontal velocity, $\bar{t} = t/\tau_h$ is the appropriately scaled time variable, and $S = N^2H^2/f^2L^2$ is the Burger number. In figure 1 the magnitude of the vertical vorticity at $x/L = \pm 0.25$ and $z/H = 0.891$ calculated to $O(\epsilon)$ using the expansion is compared to that calculated by a numerical simulation for $\epsilon = 0.02$, S=0.64, and E=1.3x10^{-4}. The figure shows that for $\bar{t} < 0.5$ both the theory and the simulation demonstrate the anticipated result: anticyclonic vorticity grows more rapidly than cyclonic vorticity. The breakdown of the theory at $x/L = 0.25$ for $\bar{t} < 0.5$ is a result of the onset of symmetric instability.

3. SYMMETRIC INSTABILITY AND FRONTOGENESIS

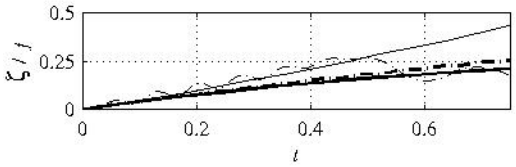

Fig. 1: Time series of the magnitude of the maximum anticyclonic vorticity at x/L=0.25 (solid and dash−dotted thin lines) and the maximum cyclonic vorticity at x/L=−0.25 (solid and dash−thick lines). The solid (dash−dotted) curves are the analytical (numerical) solution. $\epsilon = 0.02$, S=0.64, and E=1.3x10^{-4}.

Close to the location of maximum Ekman convergence the NSSU solution is prone to symmetric instability (SI). SI is a two−dimensional instability which occurs when the potential vorticity $q = -J_{xz}(m,\rho)/\rho_o$ (where J_{xz} is the Jacobian and $m = fx + v$ is the absolute momentum) is negative yet the stratification is stable and the absolute vorticity is positive, Bennetts and Hoskins 1979 (BH). The sign of q is negative if isopycnals are steeper than m−surfaces. The slope of m −surfaces are given by:

$\alpha = -(\partial m/\partial x)/(\partial m/\partial z) = -(f+\zeta)/(\partial v/\partial z)$. Hence, m−surfaces are flattest in regions of high vertical shear and low absolute vorticity. Contours of constant m, ρ , and streamfunction ψ (i.e. $u = \partial\psi/\partial z$ and $w = -\partial\psi/\partial x$) calculated using NSSU theory are plotted in figure 2.

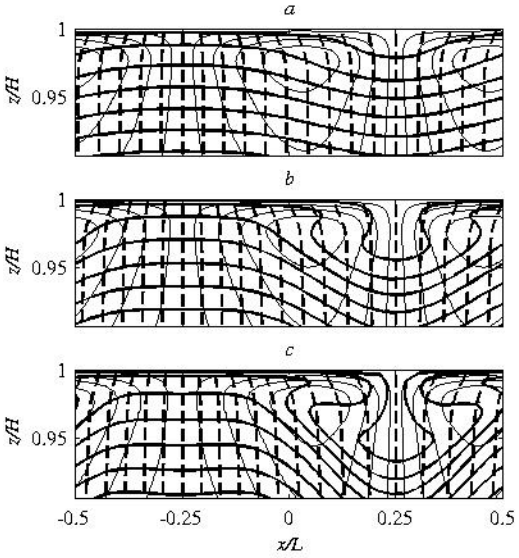

Fig. 2: NSSU solution for the density (solid thick), absolute momentum (dashed), and streamfunction (solid thin) for (a)

$\bar{t}=0.10$, (b) $\bar{t}=0.24$, and (c) $\bar{t}=0.38$. $\epsilon=0.02$, S=0.64, and E=1.3x10^{-4}.

Notice the differing structure of the m−surfaces near $x/L=\pm 0.25$. Near the location of maximum Ekman convergence (divergence) m−surfaces bow out (in) while isopycnals steepen (flatten). The bowing out of m−surfaces near $x/L=0.25$ is a consequence of both the rapid increase in the surface−intensified anticyclonic vorticity as well as the strong vertical shear in the Ekman layer. The steepening of isopycnals is due to advection. Apart from regions of density inversions, it is clear that zones of Ekman convergence tend to generate negative q by steepening isopycnals while flattening m −surfaces. This leads to symmetric instabilities which were evident in numerical simulations (figure 3). For this experiment ($\epsilon=0.02$ and S=1.00, E=10^{-4}), the deviation of the streamfunction from the NSSU solution ψ' develops two dipole vortices which are expressions of the symmetric instabilities.

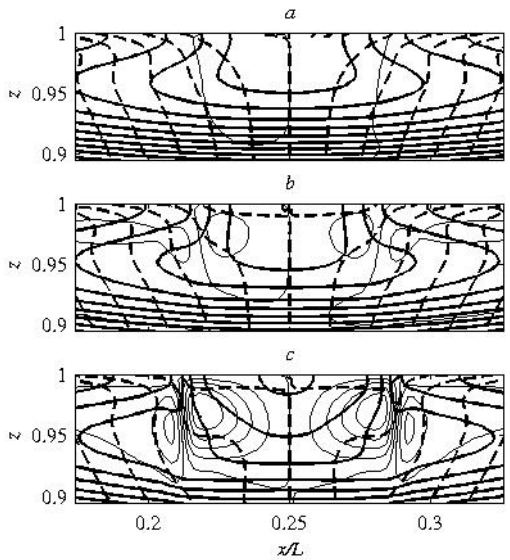

Fig. 3: Numerical simulation's solution for the density (solid thick), absolute momentum (dashed), and ψ' (solid thin) for (a) $\bar{t}=0.50$, (b) $\bar{t}=0.58$, and (c) $\bar{t}=0.67$. $\epsilon=0.02$, S=1.00, and E=10^{-4}.

The equation governing the dynamics of inviscid, small amplitude SI is :

$$\frac{\partial}{\partial t}\nabla^2\psi' = f\frac{\partial v'}{\partial z} - \frac{g}{\rho_o}\frac{\partial \rho'}{\partial x} \qquad (4)$$

where $\nabla^2\psi = \partial u/\partial z - \partial w/\partial x$ is the y−vorticity, g the gravitational acceleration, and primes denote the deviation from the basic state (in this case the NSSU solution), BH. The left hand side of (4) is the deviation from the thermal wind balance or the thermal wind imbalance (TWIB). BH showed that for q<0, perturbations to the y−vorticity can develop positive growth rates. Notice (5) implies that the magnitude of the TWIB must grow exponentially along with $|\nabla^2\psi'|$ as the instabilities develop. The TWIB driving the vortices with $\nabla^2\psi'<0$ for $x/L<0.25$ and $\nabla^2\psi'>0$ for $x/L>0.25$ is biased towards the buoyancy twisting term $-(g/\rho_o)\partial\rho'/\partial x$. Thus the growth of those vortices leads to a strengthening of buoyancy twisting, and hence a rapid sharpening of the density gradients, which is demonstrated by the convergence of isopycnals evident in figure 3c. This is the process by which SI leads to frontogenesis.

The growth of the SI does not continue indefinitely, but instead reaches a steady state in which nonlinear advection of y−vorticity balances the TWIB. As the SI to the left (right) of $x/L=0.25$ (see figure 3) grew, it propagated to the left (right) until it approached the location of maximum (minimum) wind−stress, at which point the nonlinear, steady balance was achieved. The structure of the leftward propagating SI once it attained a steady state balance is shown in figure 4. The streamfunction plotted in the figure includes the wind−driven component. Notice that the presence of the SI strongly distorts the flow in the Ekman layer, turning it downward at the front.

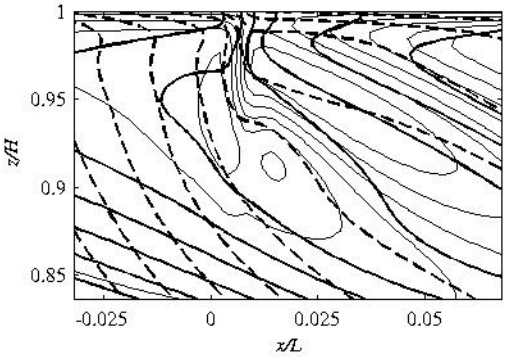

Fig. 4: Numerical simulation's solution for the density (solid thick), absolute momentum (dashed), and streamfunction (solid thin) for $\bar{t}=2.33$, $\epsilon=0.02$, S=1.00, and E=10^{-4}.

Conversely, the wind−driven circulation effects the dynamics of the SI by providing a vertical gradient in the y−vorticity (i.e.

$\partial \nabla^2 \psi / \partial z \approx \partial^2 u / \partial z^2$) which allows advection by the downwelling at the front to balance the TWIB. The two terms in this nonlinear balance:

$$J_{xz}(\psi, \nabla^2 \psi) = f \frac{\partial v}{\partial z} - \frac{g}{\rho_o} \frac{\partial \rho}{\partial x} \qquad (5)$$

are plotted in figure 5. Shaded in figure 5a (5b) is the TWIB (advection of *y*−vorticity). The color−scale is the same for both plots.

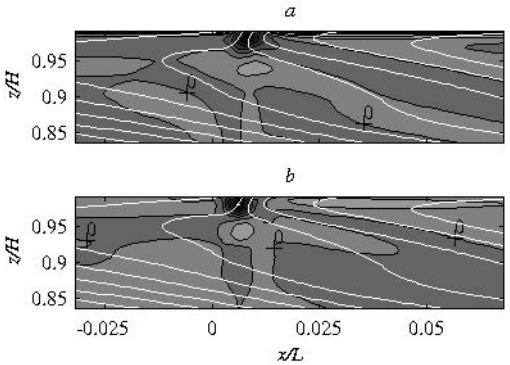

Fig. 5: Terms in the *y*−vorticity equation (5) evaluated at $\bar{t} = 2.33$: (a) the TWIB and (b) $J_{xz}(\psi, \nabla^2 \psi)$. The zero contour is labelled for both quantities and isopycnals are contoured in white.

The magnitude of both terms are strongest at the front and at the base of the Ekman layer where the buoyancy twisting and vertical advection of *y*−vorticity is largest. Both the spatial structure and magnitude of the two terms are quite similar. Thus, it is apparent that a steady solution exists for the vertical circulation about ocean fronts and that this solution crucially depends on a wind−driven circulation.

4. REFERENCES

Allen, J. S., 1973: Upwelling and coastal jets in a continuously stratified ocean. *J. Phys. Oceanogr.,* **3**, 245−257.

Bennets, D. A. and Hoskins, B. J., 1979: Conditional symmetric instability−a possible explanation for frontal rainbands. *Q. J. R. Met. Soc.,* **105**, 945−962.

Friehe, C. A., W. J. Shaw, D. P. Rogers, K. L. Davidson, W. G. Large, S. A. Stage, G. H. Crescenti, S. J. S. Khalsa, G. K. Greenhut, and F. Li, 1991: Air−sea fluxes and surface layer turbulence around a sea surface temperature front. *J. Geophys. Res.,* **96**, 8593−8609.

Halliwell, G. R., K. H. Brink, R. T. Pollard, D. L. Evans, L. A. Regier, J. M. Toole, and R. W. Schmitt, 1991: Descriptive oceanography during the Frontal Air−Sea Interaction Experiment: Medium t o large−scale variability. *J. Geophys. Res.,* **96**, 8553−8568.

Niiler, P., 1969: On the Ekman divergence in an oceanic jet. *J. Geophys. Res.,* **74**, 7048−7052.

Stern, M. E., 1965: Interaction of a uniform wind stress with a geostrophic vortex. *Deep−Sea Res.,* **12**, 355−367.

Thomas, L. N. and P. B. Rhines, 2001: Nonlinear stratified spin−up. *J. Fluid Mech.,* submitted.